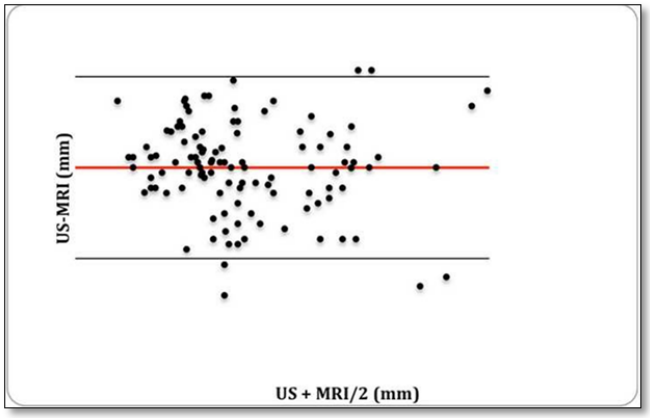

Figure 1. A Bland-Altman plot of mean values for tumor size (mm) determined by ultrasound (US) versus magnetic resonance imaging (MRI; sagittal T2-weighted) for all subjects (n=115). Mean of difference was 0.40 mm; standard deviation (SD) of difference was 0.89 mm and limits of agreements were mean -1.96 × SD=-1.38 mm and mean +1.96 × SD=2.17 mm.

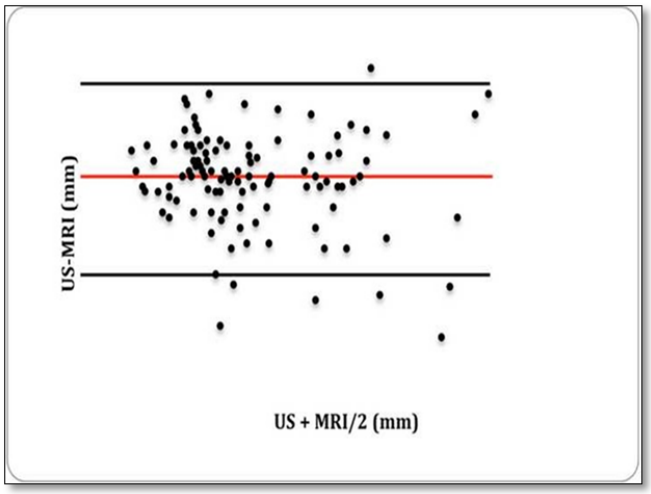

Figure 2. A Bland-Altman plot of mean values for tumor size (mm) determined by ultrasound (US) versus magnetic resonance imaging (MRI; sagittal T1-weighted) for all subjects (n=113). Mean of difference was 0.34 mm; standard deviation (SD) of difference was 0.93 mm and limits of agreements were mean -1.96 × SD=-1.51 mm and mean +1.96 × SD=2.20 mm.

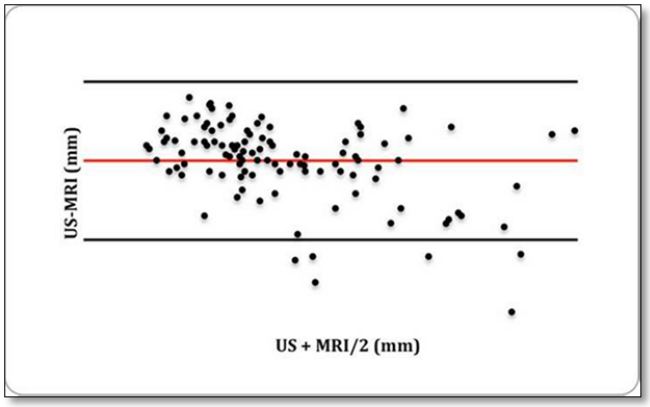

Figure 3. A Bland-Altman plot of mean values for tumor size (mm) determined by ultrasound (US) versus magnetic resonance imaging (MRI; axial T1-weighted) for all subjects (n=114). Mean of difference was 0.09 mm; standard deviation (SD) of difference was 1.07 mm and limits of agreements were mean -1.96 × SD=-2.05 mm and mean +1.96 × SD=2.22 mm.

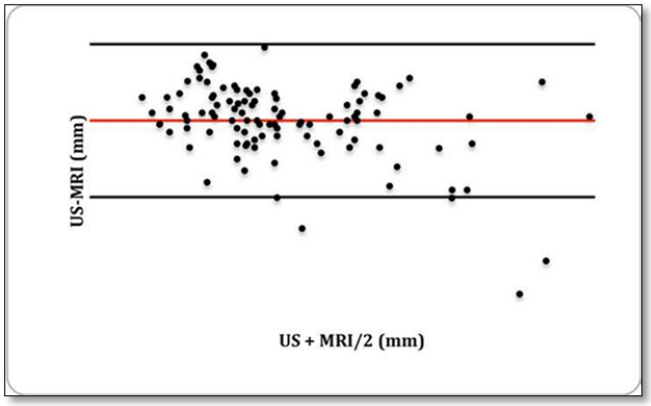

Figure 4. A Bland-Altman plot of mean values of tumor size (mm) determined by ultrasound (US) versus magnetic resonance imaging (MRI; axial T2-weighted) for all subjects (n=113). Mean of difference was 0.30 mm; standard deviation (SD) of difference was 0.99 mm and limits of agreements were mean -1.96 × SD=-1.69 mm and mean +1.96 × SD=2.28 mm.

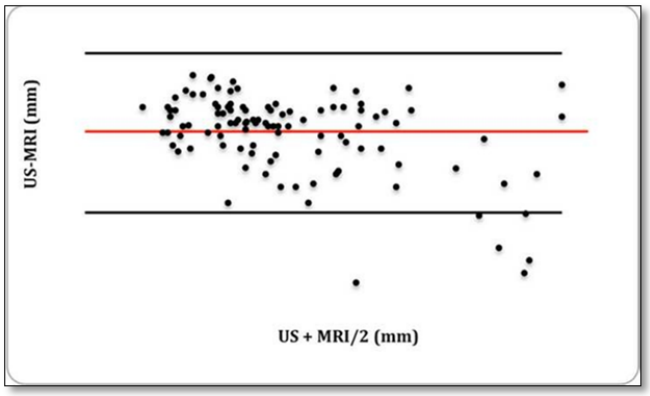

Figure 5. A Bland-Altman plot of mean values of tumor size (mm) determined by ultrasound (US) versus magnetic resonance imaging (MRI; axial gadolinium- enhanced) for all subjects (n=112). Mean of difference was -0.11 mm; standard deviation (SD) of difference was 1.25 mm and limits of agreements were mean -1.96 × SD=-2.61 mm and mean +1.96 × SD=2.39 mm.

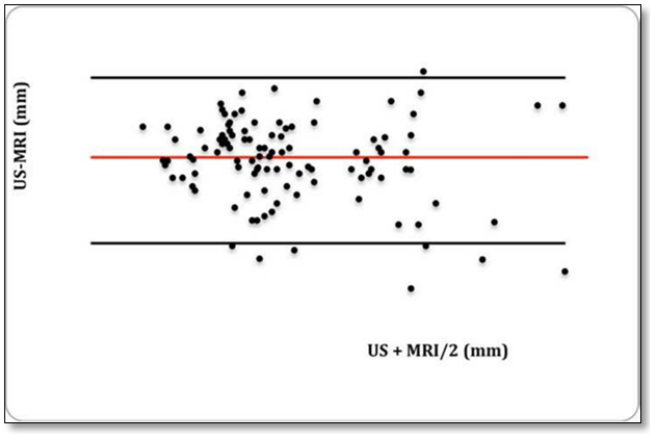

Figure 6. A Bland-Altman plot of mean values of tumor size (mm) determined by ultrasound (US) versus magnetic resonance imaging (MRI; sagittal gadolinium- enhanced) for all subjects (n=112). Mean of difference was 0.11 mm; standard deviation (SD) of difference was 0.97 mm, and limits of agreements were mean −1.96×SD=−1.84 mm and mean +1.96 × SD=2.05 mm.

Figure 7. Magnetic resonance images (A) axial and (B) sagittal T2 weighted image showing anterioposterior (height of the tumor).

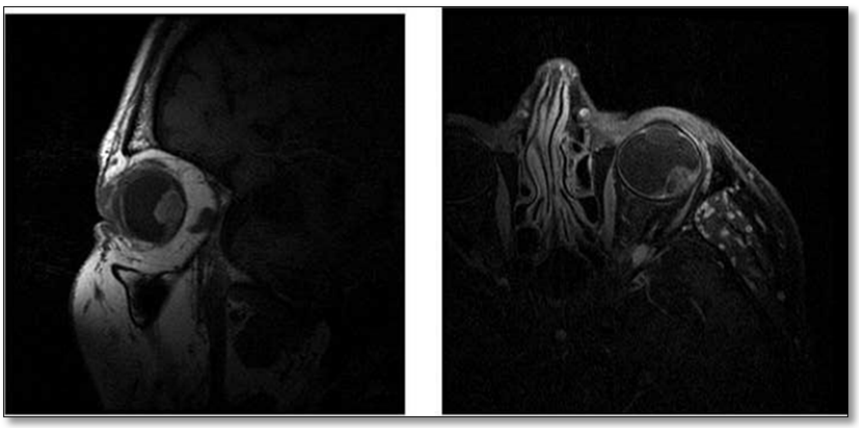

Figure 8. Magnetic resonance images (A) axial and (B) sagittal T1 weighted image with gadolinium showing anterioposterior (height of the tumor).

DISCUSSION AND CONCLUSION

Historically, CMs have been evaluated by fundoscopy and fluorescein angiography. However, ultrasonography has emerged as a gold standard for detecting and following up CM. A combination of both A-mode and B-mode ultrasonography is important. On A-scan ultrasonography, CMs show medium to low internal echoes, with or without intratum oral vascular pulsations. On B-scan, three distinct features are demonstrated: (1) an acoustic anechoic zone within a lesion of intermediate echogenicity, (2) choroidal excavation, and (3) shadowing in the orbit. When lesions are <3 cm, then images A and B mode sonography in combination is shown to give greater results [19]. There were no systematic errors in patients with tumor size <6 mm, rather a trend of MRI to underestimate ultrasound measurements without an indication of a systematic error. Above 6 mm, the measurements appeared to be less accurate; however, this error also does not appear to be systematic and rather could be indicative of measurement error. In these instances it appears that it is a larger tumor positioned on an uncommon axis, which resulted in the true tumor size not being captured between two planes of MRI measurements and significantly underestimated though this is a rare occurrence. This only becomes an issue with larger tumors when the peak of the tumor is lost between two planes or due to volume averaging, hence showing large differences between the US and MRI measurements. Overall, findings indicate that MRI is a reliable substitute for US measurements and that the axial T2 AP measurement is the most accurate within this set of MRI measurements. Future studies however will be prospective allowing for further investigation if significant differences occur between these measurements and it is recommended that the plane slices occur at 1mm intervals to minimize the risk of the peak height occurring between two planes. The advent of MR magnet advancement has given many high resolution 3D isotropic sequences which may be utilized in better segmentation and contouring of the lesions.

Magnetic resonance imaging of the orbits is an excellent modality in assessing orbital pathology. The standard practice of three orthogonal plane 3 mm fat-saturated T2-weighted images, axial and coronal T1-weighted images with fat saturations are useful in assessing melanomas.

Additional orthogonal imaging with contrast adds value in distinguishing the lesions from the uveal margins.

The MR characteristic features of melanomas are due to the paramagnetic effects of melanin, which result in shortening of T1 and T2 relaxation times [20]. This shortening effect is attributed to a combination of effects by the unpaired electrons in the free radicals and the chelated metal ions present in melanin due to dipole-dipole interactions.

The T2 hypo-intensity is probably due to the lesion's high cellularity and to the tightly cohesive bundles between cells. Other histologic features may also contribute to some degree of T2 signal heterogeneity such as hemorrhage and necrosis [21].

Given these MR considerations, CMs show hyper-intensity in relation to the cortex on T1-weighted images, hypo-intensity relative to the cortex on T2-weighted images, hyper-intensity or iso-intensity relative to the cortex on proton density-weighted imaging. These are often associated with sub-retinal hemorrhage, which is best assessed on T2-weighted images, where-in they appear as a hyper intese rim of fluid. Fat saturation techniques and paramagnetic contrast are useful to assess extra-ocular extension (Tenon's capsule and into the optic disc) and to distinguish the lesion itself from retinal detachment or hemorrhagic sub-retinal fluids [20-22].

Given the retrospective nature of our study, we were unable to obtain measurements as closely timed together as possible. Of note, these tumors are extremely slow growing and a significant change in dimension over short intervals of time may be radiologically assessed by neither ultrasonography nor MRI.

Our onus of choosing MR is that with the advent of an exponential increase in MR technology, as well as in hospital budgeting, MR is more widely available, and, more importantly, reliably reproducible. Although relatively cheaper, ultrasound examinations should be performed by skilled personnel. Further, the reproducibility of ultrasound examinations is questionable, particularly in cases of follow-up examination.

For better assessment, we recommend, in addition to the standard sequences for orbital assessment of the orbits, three-dimensional constructive interference in steady state (CISS) sequence and analysis with any commercially available reconstruction workstation software for MR protocols. Being a T2 gradient sequence, CISS gives good T2 differentiation of tumor versus the rest of the uveoscleral structures. Moreover, segmentation could be applied to calculate tumor volume. We believe this would be a better assessment of interval growth than two-plane measurement of the lesion, which is prone to error as the image acquisition planes on follow-up scans cannot be matched.

REFERENCES

1. Egan KM, Seddon JM, Glynn RJ, Gragoudas ES, Albert DM (1988) Epidemiologic aspects of uveal melanoma. Surv Ophthalmol 32:239-251.
2. Isiklar I, Leeds NE, Fuller GN, Kumar AJ (1995) Intracranial metastatic melanoma: Correlation between MR imaging characteristics and melanin content. AJR Am J Roentgenol 165: 1503-1512.
3. Byrne SF, Green RL (2002) Ultrasound of the eye and orbit. Mosby Year Book.
4. Collaborative Ocular Melanoma Study Group (2003) Trends in size and treatment of recently diagnosed choroidal melanoma, 1987-1997: Findings from patients examined at collaborative ocular melanoma study (COMS) centers: COMS report no. 20. Arch Ophthalmol 121: 1156-1162.
5. Collaborative Ocular Melanoma Study Group (1997) Factors predictive of growth and treatment of small choroidal melanoma: COMS report no. 5. Arch Ophthalmol 115: 1537-1544.
6. Collaborative Ocular Melanoma Study Group (1990) Accuracy of diagnosis of choroidal melanomas in the collaborative ocular melanoma study. COMS report no. 1. Arch Ophthalmology 108: 1268-1273.
7. Collaborative Ocular Melanoma Study Group (2003) Comparison of clinical, echographic and histopathological measurements from eyes with medium-sized choroidal melanoma in the collaborative ocular melanoma study: COMS report no. 21. Arch Ophthalmol 121: 1163-1171.
8. Shields CL, Shields JA, Perez N, Singh AD, Cater J (2002) Primary transpupillary thermotherapy for small choroidal melanoma in 256 consecutive cases: Outcomes and limitations. Ophthalmology 109: 225-234.
9. Barbazetto IA, Lee TC, Rollins IS, Chang S, Abramson DH (2003) Treatment of choroidal melanoma using photodynamic therapy. Am J Ophthalmol 135: 898-899.
10. Seddon JM, Gragoudas ES, Polivogianis L, Hsieh CC, Egan KM et al. (1986) Visual outcome after proton beam irradiation of uveal melanoma. Ophthalmology 93: 666-674.
11. Sagoo MS, Shields CL, Mashayekhi A, Freire J, Emrich J, et al. (2011) Plaque radiotherapy for juxtapapillary choroidal melanoma: Tumor control in 650 consecutive cases. Ophthalmology 118: 402-407.
12. Jampol LM, Moy CS, Murray TG, Reynolds SM, Albert DM, et al. (2002) The COMS randomized trial of iodine 125 brachytherapy for choroidal melanoma: IV. Local treatment failure and enucleation in the first 5 years

after brachytherapy. COMS report no. 19. Ophthalmology 109: 2197-2206.

13. Hawkins BS, Collaborative Ocular Melanoma Study Group (2004) The Collaborative Ocular Melanoma Study (COMS) randomized trial of pre-enucleation radiation of large choroidal melanoma: IV. Ten year mortality findings and prognostic factors. COMS report number 24. Am J Ophthalmol 138: 936-951.
14. Emara K, Weisbrod DJ, Sahgal A, McGowan H, Jaywant S, et al. (2004) Stereotactic radiotherapy in the treatment of juxtapapillary choroidal melanoma: Preliminary results. Int J Radiat Oncol Biol Phys 59: 94-100.
15. Krema H, Somani S, Sahgal A, Xu W, Heydarian M, et al. (2009) Stereotactic radiotherapy for treatment of juxtapapillary choroidal melanoma: 3 year follow-up. Br J Ophthalmol 93: 1172-1176.
16. Nag S, Quivey JM, Earle JD, Followill D, Fontanesi J, et al. (2003) The American Brachytherapy Society recommendations for brachytherapy of uveal melanomas. Int J Radiat Oncol Biol Phys 56: 544-555.
17. Müller-Forell W, Wibke S (2003) Imaging of orbital and visual pathway pathology. Springer-Verlag Berlin Heidelberg.
18. Peyster RG, Augsburger JJ, Shields JA, Satchell TV, Markoe AM, et al. (1985) Choroidal melanoma: Comparison of CT, fundoscopy and US. Radiology 156: 675-680.
19. Mafee MF, Peyman GA, McKusick MA (1985) Malignant uveal melanoma and similar lesions studied by computed tomography. Radiology 156: 403-408.
20. Hosten N, Bornfeld N, Wassmuth R, Lemke AJ, Sander B, et al. (1997) Uveal melanoma: Detection of extra ocular growth with MR imaging and US. Radiology 202: 61-67.
21. Mafee MF (1998) Uveal melanoma, choroidal hemangioma and simulating lesions. Role of MR imaging. Radiol Clin North Am 36: 1083-1099.
22. Houle V, Belair M, Allaire GS (2011) AIRP best cases in radiologic-pathologic correlation: Choroidal melanoma. Radiographics 31: 1231-1236.